Chemical Geology 251 (2008) 112–119

Contents lists available at ScienceDirect

Chemical Geology

journal homepage: www.elsevier.com/locate/chemgeo

Fluorapatite solubility in H_2O and H_2O–NaCl at 700 to 900 °C and 0.7 to 2.0 GPa

Angelo Antignano [1], Craig E. Manning *

Department of Earth and Space Sciences, University of California, Los Angeles, CA, 90095-1567, USA

ARTICLE INFO

Article history:
Received 1 November 2007
Received in revised form 3 March 2008
Accepted 4 March 2008

Editor: J. Fein

Keywords:
Apatite solubility
Experimental petrology
Brines
REE mobility
Metamorphic fluids

ABSTRACT

The solubility of Durango fluorapatite was measured in H_2O and H_2O–NaCl at 700–900 °C and 0.7–2.0 GPa in a piston-cylinder apparatus. Solubility was determined by weight loss using a double-capsule method. At all conditions, fluorapatite dissolves incongruently to monazite+fluid, but residual monazite crystals were below weighing detection limits of 0.6 μg. The concentration of fluorapatite dissolved in pure H_2O is low at all investigated conditions (56±8 to 288±8 ppm by weight), but increases with temperature (T) and pressure (P). The data are well described by the equation $\log c^{\circ}_{ap} = -3.56 + .00241T + 9.17 \log\rho_{H_2O}$, where c°_{ap} is apatite concentration in H_2O (in ppm), T is in Kelvin, and ρ_{H_2O} is H_2O density in g cm^{-3}. Fluorapatite solubility was also measured in H_2O–NaCl fluids at a range of P and T. Results indicate a strong increase in dissolved fluorapatite concentration with rising NaCl mole fraction (X_{NaCl}) at all P and T, and X_{NaCl} to near halite saturation. The data were fit to the equation $c_{ap} = c^{\circ}_{ap} + Ba^{1/2}_{NaCl}$ where c_{ap} is apatite concentration in H_2O–NaCl (in ppm), a_{NaCl} is NaCl activity calculated from an ideal mixing model for H_2O–NaCl, and $B = (4.4 + 1.1P^4)\exp(0.0070T)$, with P in GPa, and T in Kelvin. The results differ from previous work in that the newly determined solubilities are ≥10 times lower at comparable conditions, increase with P at constant T, and show a strong positive correlation with X_{NaCl}. The discrepancy is attributed to unrecognized growth of new apatite crystals at run conditions in the earlier study. Compared to fluorite, calcite and anhydrite, fluorapatite solubility is significantly lower in H_2O and H_2O–NaCl; however, the solubility enhancement by NaCl relative to that in pure H_2O is similar to anhydrite and much greater than calcite and fluorite. The NaCl enhancement of solubility increases with T but decreases with P. The undetectable weight of monazite requires significant solubility of light rare-earth elements (LREE), likely as chloride complexes, and indicates that metasomatic interaction of brines with apatite-bearing rocks at high metamorphic grades can mobilize substantial LREE.

1. Introduction

Apatite ($Ca_5(PO_4)_3(OH,F,Cl)$) is a ubiquitous accessory mineral in igneous and metamorphic rocks that is widely used to evaluate petrogenetic processes (e.g., Piccoli and Candela, 2002; Spear and Pyle, 2002). As an important reservoir for rare-earth elements (REE), apatite carries information about magmatic source characteristics or metamorphic protolith (Nagasawa, 1970; Gromet and Silver, 1983; Fleischer and Altschuler, 1986; Sorensen and Grossman, 1989; Fleet and Pan, 1995a,b). Apatite's relatively high U content makes it a useful phase for geochronology over a wide range of conditions (Harrison et al., 2002; Farley and Stockli, 2002; Gleadow et al., 2002). In addition, OH, F and Cl in its c-axis channels can be used to constrain fluid composition and equilibration temperature (Korzhinskiy, 1981; Yardley, 1985; Zhu and Sverjensky, 1991, 1992; Piccoli and Candela, 1994; Boyce and Hervig, 2008), while minor concentrations of other volatiles (e.g., C, N, S, Br, I, B; Pan and Fleet, 2002) offer opportunities to monitor a wide range of fluid processes attending mineral equilibration.

Apatite is particularly suitable for assessing the role of fluids at high pressures, where metasomatic activity is important but poorly understood. In subduction-zone settings, apatite in vein assemblages and as a daughter mineral in fluid inclusions testifies to the mobility of its essential constituents in high-pressure fluids (Barnicoat, 1988; Selverstone et al., 1992; Philippot and Selverstone, 1991; Bebout and Barton, 1993; Giaramita and Sorensen, 1994; FernandezCaliani et al., 1996; Franz et al., 2001; Gao and Klemd, 2001; Torok, 2001; Xu et al., 2001; Glodny et al., 2003; Rubatto and Hermann, 2003; Gao et al., 2007). Apatite has also been used to gain insight into metasomatic processes in high-grade amphibolites and granulites (e.g., Pan and Fleet, 1996; Harlov and Förster, 2002; Harlov et al., 2002; Harlov and Förster, 2003), as well as the mantles of Earth and other terrestrial planets (Nash and Hausel, 1973; O'Reilly and Griffin, 2000; Patiño Douce and Roden, 2006).

An important first step in using apatite to monitor elemental mass transfer in high-pressure settings is the determination of its solubility in geologic fluids; however, experimental results give problematic results. Ayers and Watson (1991) reported solubilities in pure H_2O at 800–1200 °C and 1–3 GPa that were relatively high (500–4400 ppm) and generally increased with rising temperature. But they also reported decreasing solubility with increasing pressure and no change with the addition of NaCl. This behavior contrasts with that of other Ca

* Corresponding author. Tel.: +1 310 206 3290; fax: +1 310 206 8995.
E-mail address: manning@ess.ucla.edu (C.E. Manning).
[1] Current address: Exxon Mobil Corporation, PO Box 4778, Houston, TX, 77210-4770, USA.

0009-2541/$ – see front matter © 2008 Elsevier B.V. All rights reserved.
doi:10.1016/j.chemgeo.2008.03.001

salts such as calcite, fluorite and anhydrite, for which pressure and NaCl promote greater solubility (Newton and Manning, 2002, 2005; Tropper and Manning, 2007b).

In an effort to identify the cause of apparent differences in apatite solubility behavior relative to that of similar minerals, and to extend solubility measurements to aid study of deep fluid–rock interaction, we undertook a systematic investigation of the solubility of fluorapatite in H_2O and H_2O–NaCl at high pressure (P) and temperature (T). We hypothesized that Ayers and Watson (1991) encountered growth of new apatite crystals which could explain some of the patterns in their data. Accordingly, we established methods for ensuring that growth of these new crystals was suppressed. In addition, with the new results in pure H_2O as a foundation, we also conducted experiments on fluorapatite solubility in H_2O–NaCl fluids. Taken together, the new data allow assessment of fluorapatite solubility in some model metamorphic and igneous fluids of the lower crust and upper mantle.

2. Experimental methods

Experiments were conducted on inclusion-free, gem-quality fluorapatite from Durango, Mexico, which contains ~3.5 and ~1 wt.% F and LREE, respectively (Young et al., 1969). Small chips were first ground into ~1-mm long ellipsoids using 240-grit emery paper to remove sharp edges, and then rolled in 400-grit paper until they acquired a polish. The polished grains were cleaned in ultra-pure H_2O in an ultrasonic bath, and then dried at 400 °C for 15 min. This procedure generated crystals that ranged in weight from 1 to 5 mg. For each experiment, a single crystal was loaded into a protective 1.6 mm OD by 6 mm long Pt tube and crimped. The capsule was then placed in a 3.5 mm OD Pt tube with ultra-pure H_2O ± reagent-grade NaCl. Each capsule was sealed by arc-welding, and then placed in a 115 °C oven for 1 h to test for leakage. Capsules showing weight loss were not used. The double-capsule method is advantageous for several reasons: the inner capsule contains the crystals if they break, which permits solubility determination from weight changes of the bulk inner capsule containing the fragments; it segregates crystals from most of the fluid, which minimizes back-reaction during quench; and it acts as a thermal baffle to reduce temperature gradients during the experiment.

The experiments were conducted in a piston-cylinder apparatus, using 2.54-cm-diameter NaCl-graphite assemblies and the piston-out method (Manning, 1994; Manning and Boettcher, 1994). Conditions were 0.7–2.0 GPa and 700–900 °C. Temperature was controlled using calibrated Pt-$Pt_{10}Rh_{90}$ thermocouples, with no correction for the effect of pressure on emf. The accuracy of the reported temperature is estimated to be ±3 °C. Pressure was monitored using a Heise gauge and maintained to within 200 bar gauge pressure. Quenching was achieved by cutting power to the apparatus, which cooled the experiments to ≤50 °C within 1 min (Manning and Boettcher, 1994).

After each experiment, the H_2O content was checked by recording the weight loss associated with puncturing and drying the outer capsule at 115 °C for 15 min and then 300 °C for 15 min; H_2O mass balance in all cases was better than 0.8%. The apatite grain was extracted from the inner capsule, treated ultrasonically in ultra-pure H_2O to remove adhering quench precipitate, dried in air at 115 °C, and then weighed. In several cases, the crystal broke during ultrasonic treatment; these experiments were discarded. All run products were inspected at low magnification using a binocular microscope. Grains from selected experiments were mounted and characterized by scanning electron microscope (SEM).

Fluorapatite solubility is reported in parts/million by weight (ppm, calculated from the crystal weight loss divided by the mass of H_2O + NaCl + crystal weight loss), because of the mixed solvent and the complex composition of the natural material used. As noted below, trace monazite was produced by incongruent fluorapatite dissolution, but its weight was negligible and was ignored. Reported NaCl mole fractions (X_{NaCl}) were calculated from the starting ratio $n_{NaCl}/(n_{NaCl}+n_{H_2O})$ in the experiment; that is, they neglect dissolved fluorapatite. Weights were determined on a Mettler M3 microbalance or Mettler UMX2 ultra-microbalance with weighing errors of $1\sigma=2$ and $1\sigma=0.2$ μg, respectively, determined by repeated weighings of a standard over the course of this study. Reported uncertainties are propagated 1σ weighing errors. Minimum detection limit using the UMX2 is assumed to be 3σ, or 0.6 μg. The compositions of newly formed crystals in this study were not determined quantitatively, so they are referred to below as "apatite"; we reserve "fluorapatite" for the Durango starting material.

3. Results

3.1. Textures

Run products included three kinds of apatite, as well as monazite. The apatite crystal types were: (1) large, residual, partially dissolved starting fluorapatite grains; (2) hollow, acicular apatite needles; and

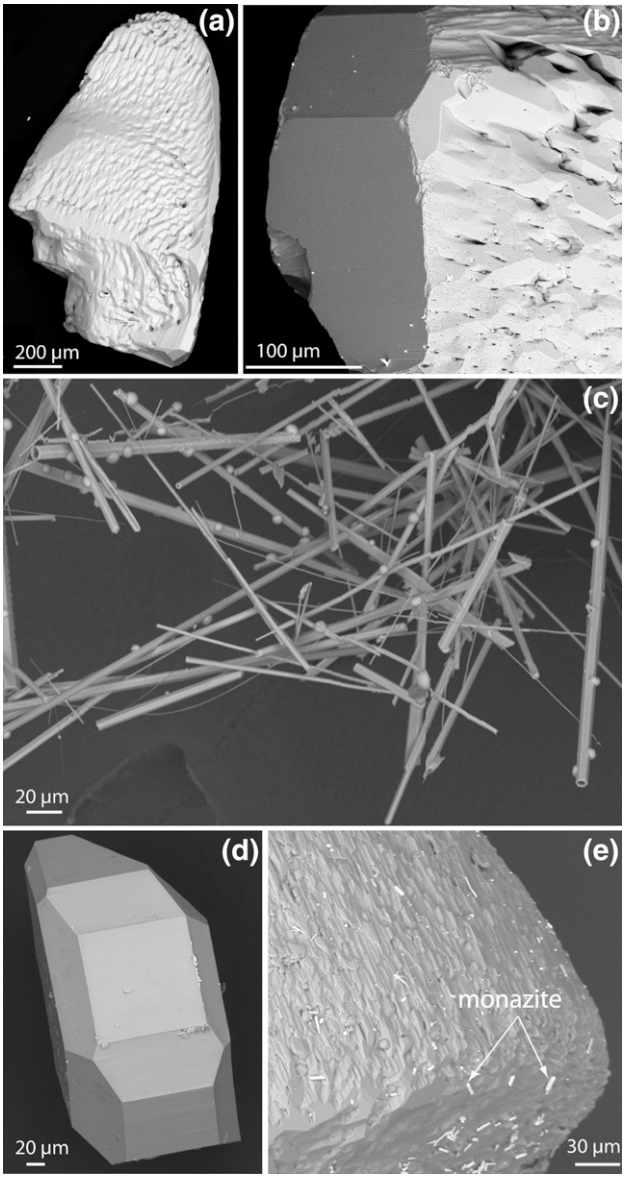

Fig. 1. SEM images of run products from selected experiments. (a, b) Residual fluorapatite crystals illustrating solution-rounded edges, dissolution grooves, etch pits, and newly grown facets. (c) Hollow apatite needles which nucleate primarily in the outer capsule upon quench. (d) Euhedral vapor-transport crystal of apatite which nucleated in the outer capsule during the experiment. (e) Micron-scale monazite crystals (high intensity) on the surface of partly dissolved starting fluorapatite.

(3) equant, euhedral, newly formed apatite grains in the outer capsules of some experiments. Residual starting crystals exhibited textures consistent with partial dissolution and new growth, including grooves, pits, tubes and new facets (Fig. 1a,b). New crystal faces developed on the tops and tips of crystals, whereas the bases of grains, which were in contact with the capsule, show only dissolution textures.

The second type of apatite crystal was hollow, acicular needles (Fig. 1c) which were distributed randomly throughout inner and outer capsules. Their abundance increased with increasing *T*, *P*, and X_{NaCl} (i.e., expected solubility). The crystals were up to 200 μm in the longest dimension and ranged from sparse crystallites to dense fibrous mats. Because of their morphology, high nucleation density and abundance, we interpret these crystals to be quench material.

The third apatite morphology, which occurred only in some run products, was euhedral, blocky crystals up to ~300 μm in the longest dimension and found in the outer capsule. Their formation did not depend on *T*, *P*, or NaCl concentration. These crystals were easily distinguished from apatite needles and residual crystals by their distinct morphology (Fig. 1d). The large size, sporadic nature, low nucleation density, and occurrence only in the outer capsules suggest that these crystals grew at high *P* and *T* during the runs. Similar crystals have been identified in solubility studies of other refractory oxides in H_2O, including calcite, rutile and corundum (Caciagli and Manning, 2003; Tropper and Manning, 2005, 2007a). These grains are termed "vapor-transport crystals" (VTC) and, given appropriate conditions (e.g., time, unavoidable temperature gradients of order 1 °C, inner capsule orientation), they may nucleate and grow in the outer capsule. Vapor-transport crystals represent the dissolution and reprecipitation of the apatite starting material. Experiments in which VTC grew were discarded because it proved impossible to account accurately for weight change of fluorapatite in these cases.

Our interpretations of the origin of quench and transport crystals are consistent with the results of Wyllie et al. (1962), who found that apatite habit varied with conditions of formation. Apatite synthesized at subsolidus conditions in their experiments exhibited a stubby hexagonal prismatic morphology with a maximum elongation ratio of 3:1, similar to our transport crystals. Apatite precipitated on quench had an acicular morphology with elongation of up to 20:1 parallel to the *c*-axis. Wyllie et al. (1962) reported that quench apatite was commonly hollow, with the cavity running the length of the crystal, similar to our quench crystals.

In addition to the three apatite morphologies, we also observed <5 μm grains of monazite on the surfaces of fluorapatite starting crystals (Fig. 1e). Monazite is interpreted to result from incongruent dissolution of the REE-bearing natural fluorapatite starting material in H_2O, or H_2O+NaCl, to (REE)PO_4+dissolved solutes. Similar incongruent dissolution of Durango fluorapatite to monazite was observed by Harlov and Förster (2003) and Harlov et al. (2005). To evaluate the contribution of residual monazite to the measured weight change, selected fluorapatite crystals from the full range of NaCl concentrations investigated were weighed and then mounted uncoated for SEM imaging to record monazite distribution and texture. The crystals were then placed in an ultrasonic bath with distilled H_2O to dislodge the monazite. After drying and reweighing, the crystals were imaged a second time. No monazite was observed on the fluorapatite surfaces, indicating that ultrasonic treatment completely removed the monazite grains. No weight changes were detected using the high-precision balance. The weight of residual monazite was therefore neglected in all solubility calculations; however, all results strictly reflect the solubility of fluorapatite+monazite.

3.2. Equilibrium

Initial experiments were conducted for 48 h. New growth on the surfaces of the ellipsoidal fluorapatite starting material was observed at all conditions investigated, indicating significant reaction between apatite and solution (Fig. 1a, b); however, transport crystals nucleated in all these runs (Fig. 1d). Reduction of run durations to 24 h resulted in no transport crystals, with the exception of two runs at 900 °C; these latter experiments were omitted from the data set. Similar studies on anhydrite and fluorite, which also employed the double-capsule method, demonstrated that 24 h were sufficient for

Table 1
Experimental results

Run number	*T* (°C)	*P* (GPa)	NaCl (mg)	H_2O (mg)	X_{NaCl}	Apatite in (mg)	Apatite out (mg)	Solubility (ppm)
700AP-5	700	1.0	0.000	35.744	0.000	1.9229	1.9209	56(8)
700AP-7	700	1.0	41.407	29.289	0.304	1.1251	0.9667	2236(4)
700AP-8	*700*	*1.0*	*34.205*	*11.128*	*0.42(03)*	*0.7442*	*0.6248*	*2627(6)*
7AP-7	800	0.7	0.000	35.027	0.000	2.2531	2.2500	88(8)
7AP-5	800	0.7	15.193	36.214	0.114	4.153	4.083	1360(55)
7AP-2	800	0.7	37.257	25.487	0.310	3.294	3.047	3921(45)
7AP-6	800	0.7	33.005	10.657	0.487	1.248	0.999	5671(64)
800AP-6	800	1.0	0.000	35.519	0.000	0.7890	0.7868	62(8)
800AP-7	800	1.0	7.394	36.132	0.059	0.8760	0.8265	1136(7)
800AP-5	800	1.0	19.564	30.810	0.163	5.192	5.033	3146(56)
800AP-9	800	1.0	36.891	27.654	0.291	1.0775	0.8083	4153(4)
800AP-10	800	1.0	54.609	16.146	0.510	0.6150	0.1563	6441(4)
15AP-12	800	1.5	0.000	35.614	0.000	1.3927	1.3857	197(8)
15AP-1	800	1.5	3.998	28.306	0.042	4.349	4.288	1885(87)
15AP-2	800	1.5	7.265	30.707	0.068	7.632	7.531	2653(74)
15AP-14	800	1.5	34.561	24.618	0.302	2.1676	1.6315	8978(5)
20AP-2	800	2.0	0.000	35.664	0.000	5.272	5.250	616(79)
900AP-7	900	1.0	0.000	36.194	0.000	2.6133	2.6099	94(8)
900AP-8	900	1.0	0.000	40.881	0.000	1.4045	1.4012	81(7)
900AP-1	900	1.0	4.279	35.729	0.036	4.613	4.541	1796(71)
900AP-4	900	1.0	20.765	30.660	0.172	5.130	4.843	5550(55)
900AP-5	900	1.0	25.906	17.338	0.313	4.247	3.811	9982(65)
900-15-AP-1	900	1.5	0.000	36.129	0.000	1.6369	1.6265	288(8)
900-15-AP-13	900	1.5	30.658	27.416	0.256	1.1822	0.2771	15346(5)
900-15-AP-3	900	1.5	31.016	10.806	0.467	1.3186	0.3227	23259(9)

Italics indicate experiment 700AP-8 at halite saturation, with X_{NaCl} from Aranovich and Newton (1996) and Koster van Groos (1991); "in" and "out" refer respectively to the weights before and after the experiment. Weights reported to three decimal places were determined on a Mettler M3 microbalance (1σ=2 μg); those to four places were determined on a Mettler UMX2 ultra-microbalance (1σ=0.2 μg). Parenthetical numbers reflect 1σ uncertainty in final digits, based on propagation of weighing errors.

equilibrium (Newton and Manning, 2005; Tropper and Manning, 2007b).

3.3. Fluorapatite solubility in H_2O

Experimental results are presented in Table 1 and Fig. 2. With one exception, the data indicate that fluorapatite solubility in pure H_2O rises with increasing P and T. At 800 °C, fluorapatite solubility increases by about one order of magnitude, from 61 ± 8 ppm at 1.0 GPa to 616 ± 79 at 2.0 GPa (Fig. 2a). A similar trend of rising solubility with increasing P is observed at 900 °C (Fig. 2b). At 1.0 and 1.5 GPa, fluorapatite solubility increases with increasing T (Fig. 2b). The one exception to the general trends exhibited by the data set is the 88 ± 8 ppm solubility measured in experiment 7AP-7 (800 °C, 0.7 GPa; Table 1), which is higher than the value at 1.0 GPa at the same T. No evidence for vapor-transport was found in this experiment, but it is possible that the crystal chipped during post-run handling. This experiment was omitted from further consideration.

We derived an empirical relation describing the logarithm of fluorapatite solubility in pure H_2O, c°_{ap}, as a function of T and H_2O density (Manning, 1994, 1998; Caciagli and Manning, 2003). Because there are relatively few data points in the present study, we assumed linear dependence of log c°_{ap} on T at 1.0 GPa and at $\rho_{H_2O} = 1$, which gave

$$\log c^{\circ}_{ap} = -3.56 + 0.00241T + 9.17\log\rho_{H_2O} \quad (1)$$

(Fig. 2c) where c°_{ap} is in ppm, T is in Kelvin and ρ_{H_2O} is H_2O density in g cm^{-3} (Haar et al., 1984). As noted above, run 7AP-7 was omitted from the fit. Predicted solubility in H_2O using Eq. (1) yields an average deviation of ±10% relative and is shown in Fig. 2.

3.4. Fluorapatite solubility in H_2O–NaCl

Fluorapatite solubility rises with increasing X_{NaCl} at all conditions investigated (Fig. 3). In general, the enhancement of solubility is greatest at low X_{NaCl} (less than ~0.1) and becomes less pronounced at higher NaCl concentrations. The experiment at 700 °C, 1.0 GPa, had starting bulk fluid composition of $X_{NaCl} = 0.49$ (7AP-6, Table 1). Because this composition is predicted to be supersaturated with respect to halite at run conditions (Koster van Groos, 1991; Aranovich and Newton, 1996), X_{NaCl} was adjusted to predicted halite saturation of 0.42 ± 0.03.

At each P and T investigated, fluorapatite solubility was found to vary linearly in the square root of NaCl activity (a_{NaCl}), as determined from the ideal-solution model of Aranovich and Newton (1996, their Eq. (4)). The data were fit using the equation

$$c_{ap} = c^{\circ}_{ap} + Ba^{1/2}_{NaCl} \quad (2)$$

where

$$B = (4.4 + 1.1P^4)\exp(0.007T) \quad (3)$$

and c_{ap} is in ppm, T is in Kelvin and P is in GPa. Eqs. (1)–(3) yield an average absolute deviation of 9%, with misfit normally distributed about zero and no systematic deviations with P, T or X_{NaCl}.

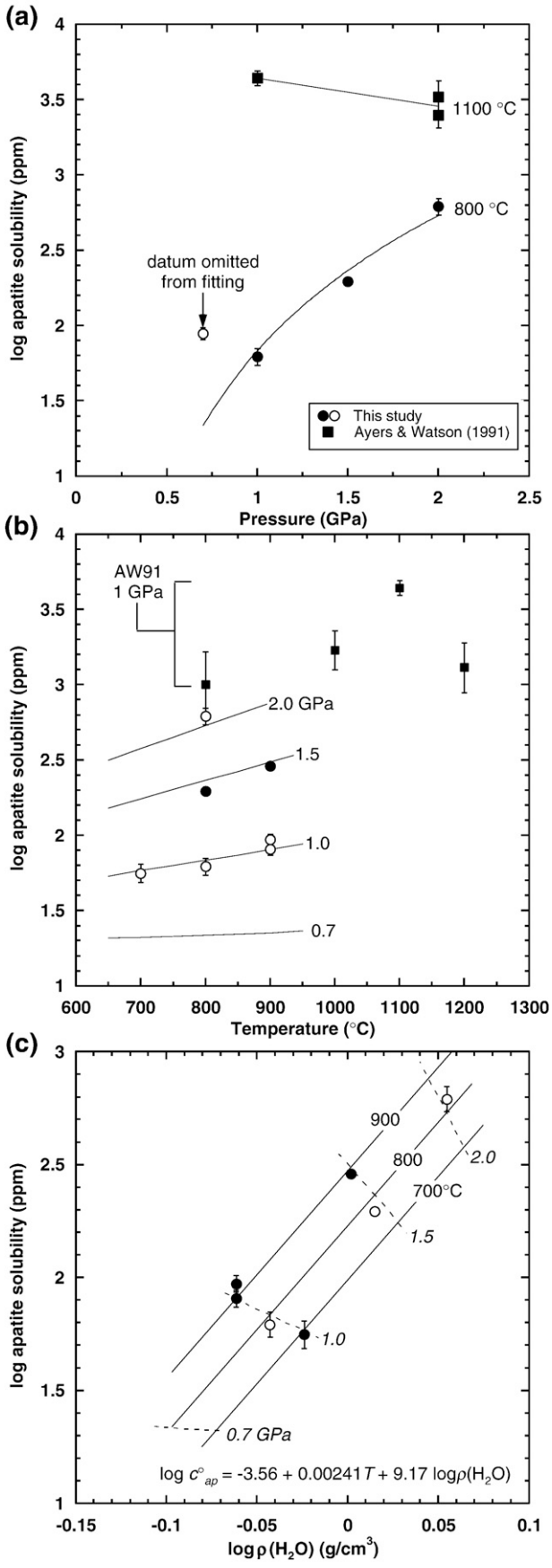

Fig. 2. (a) Variation in fluorapatite solubility in H_2O with P. Data from this study are from the experiments at 800 °C (open circle shows datum ignored in fitting). Solid curve determined from Eq. (1). Results of Ayers and Watson (1991) at 1100 °C shown for comparison. (b) Variation in apatite solubility in H_2O with T. Data from this study are from the experiments shown with circles (800 °C, 0.7 GPa datum ignored). Solid curves determined from Eq. (1). Results of Ayers and Watson (1991) at 1 GPa shown for comparison. (c) Variation in fluorapatite solubility with H_2O density (Haar et al., 1984). Solid lines are isotherms, dashed lines are isobars, both calculated from Eq. (1). All errors 1σ.

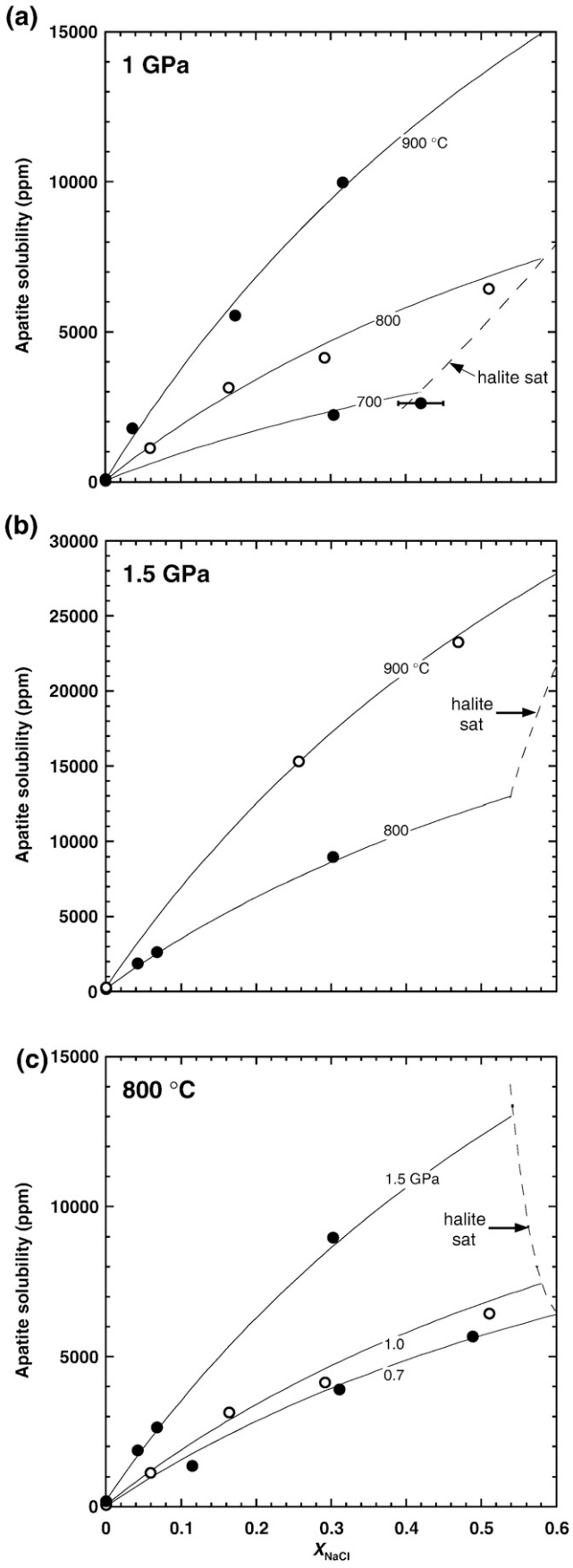

Fig. 3. Fluorapatite solubility vs. X_{NaCl} showing (a) variation with T at 1 GPa, (b) variation with T at 1.5 GPa, and (c) variation with P at 800 °C. Curves calculated from Eqs. (1)–(3). Halite saturation estimated from Aranovich and Newton (1996). All errors 1σ.

4. Discussion

4.1. Comparison to previous results

The results of this study differ from those of Ayers and Watson (1991) in three significant ways. First, Ayers and Watson (1991) report fluorapatite solubilities in pure H_2O that are about an order of magnitude greater at 1 GPa (Fig. 2b). Second, their results suggest that at constant T, solubility decreases with increasing P (Fig. 2a), whereas our data indicate an increase with P. Finally, they report no change in solubility in the presence of H_2O–NaCl fluids; however, we find a strong and systematic variation with X_{NaCl} (Fig. 3). Ayers and Watson (1991) also used Durango fluorapatite in their experiments, so the differences are not due to apatite composition. They did not note monazite as an incongruent reaction product, but its small mass in our experiments cannot account for the differences.

We attribute the discrepancies between our results and those of Ayers and Watson (1991) to the differing interpretations of run products in the respective studies. Tropper and Manning (2005) showed that a parallel study of rutile solubility by Ayers and Watson (1993b), which employed the same methods as Ayers and Watson (1991), gave solubilities that were too high due to the misinterpretation of vapor-transport crystals as quench products. Ayers and Watson (1991) noted apatite "recrystallization" in one experiment but did not discuss quench textures; however, Ayers and Watson (1993a) observed new apatite crystals which they interpreted to have formed during quenching. Three considerations suggest that a fraction of these crystals in the experiments of Ayers and Watson (1991) could be VTC. First, failure to collect and incorporate VTC will result in apparent solubility that is systematically too high, consistent with the fact that the results of Ayers and Watson (1991) yield or would predict greater solubility than we observed. Second, the sporadic nature of transport-crystal nucleation that we observed would explain the lack of a systematic trend with increasing T at 1 GPa in the study of Ayers and Watson (1991) (Fig. 2b). Finally, a greater tendency to produce VTC is expected in the earlier work due to the ~5 °C temperature gradients in the capsules, which were ~8 mm in length and placed vertically in the experimental assembly (Ayers et al., 1992). In contrast, the present study used horizontally placed, 3.5 mm O.D. capsules (post-run vertical dimension is typically ~2.5 mm), with an additional inner capsule, which should reduce vertical T gradients. Considering that VTC grew in some of our 24-h experiments at 900 °C — even with a geometry designed to minimize temperature gradients — it seems likely that the generally higher experimental T and less favorable geometry conspired to produce undiagnosed VTC in the study of Ayers and Watson (1991).

4.2. Comparison to other minerals

At similar P and T, fluorapatite solubility in pure H_2O is lower than that of the other Ca salts that have been studied, which include calcite ($CaCO_3$), fluorite (CaF_2) and anhydrite ($CaSO_4$). This is exemplified by comparison with previous experiments at 1 GPa. At this P, fluorite solubility increases from 710 ppm at 700 °C to 1800 ppm at 900 °C (Tropper and Manning, 2007b), which is 10–20 times greater than fluorapatite at the same conditions. Anhydrite solubility is higher still, increasing from 2600 to 3800 ppm at 700–800 °C (Newton and Manning, 2005), or ~50–60 times above fluorapatite. Calcite solubility at 700 °C is similar to anhydrite (Caciagli and Manning, 2003), but melting in the system $CaCO_3$–H_2O complicates the comparison at higher T. The low solubility of fluorapatite in pure H_2O demonstrates that it is the most refractory of the Ca salts commonly found in high-grade metamorphic rocks VTC in some 24-h experiments at 900 °C, if pore fluids are very dilute aqueous solutions.

As with the other Ca salts, fluorapatite solubility increases with addition of NaCl to H_2O. Fig. 4 compares the solubility behavior of

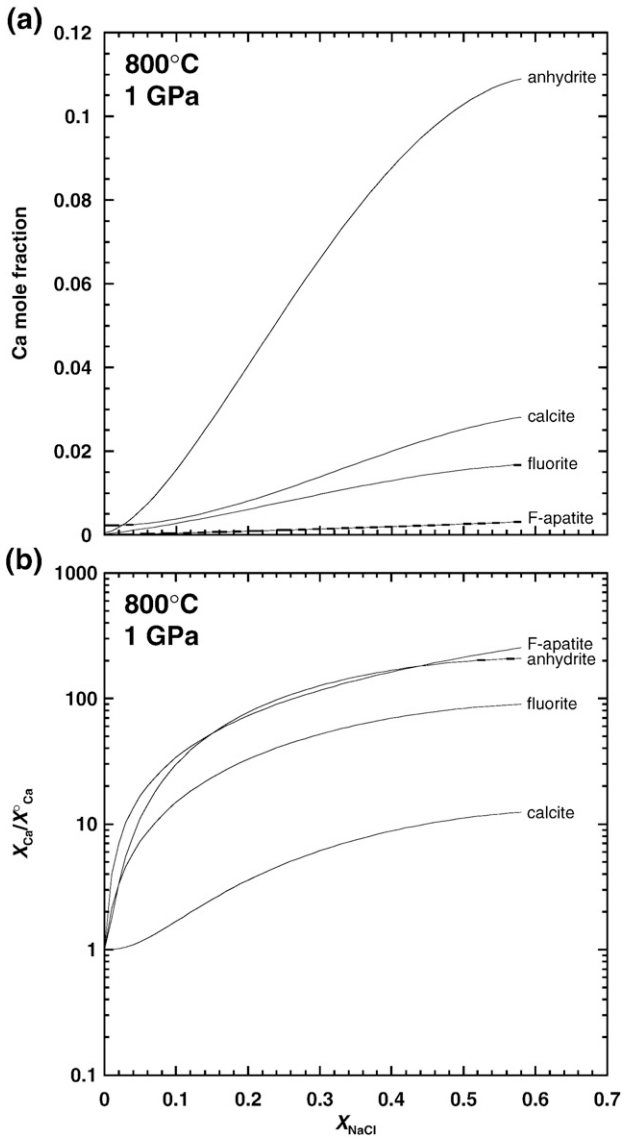

Fig. 4. Comparison of the predicted solubility of fluorapatite (this study, Eqs. (1)–(3)) with that of fluorite (Tropper and Manning, 2007b), calcite (Newton and Manning, 2002) and anhydrite (Newton and Manning, 2005) at 800 °C, 1 GPa. (a) Comparison of solubility calculated as mole fraction of Ca in solution. (b) comparison of the enhancement of solubility, as determined from the ratio of predicted solubility (X_{Ca}) divided by that in H_2O (X_{Ca}°).

fluorapatite at 800 °C, 1 GPa, to calcite, fluorite and anhydrite (Newton and Manning, 2002, 2005; Tropper and Manning, 2007b). For this comparison the concentration scale was transformed to mole fraction, assuming for simplicity that fluorapatite composition is stoichiometric $Ca_5(PO_4)_3F$. As with the other Ca-bearing minerals, Ca mole fraction in fluorapatite-equilibrated H_2O–NaCl fluid rises with increasing NaCl concentration (Fig. 4a). However, Ca solubility at fluorapatite saturation is much lower than in fluids coexisting with anhydrite, calcite or fluorite at any X_{NaCl} at 800 °C, 1 GPa. The effect of NaCl on solubility can be assessed from the ratio X_{Ca}/X°_{Ca} where X°_{Ca} is the Ca mole fraction in pure H_2O. Fig. 4b shows that NaCl enhances the solubility of fluorapatite to an extent similar to anhydrite, and to a much greater degree than calcite and fluorite.

Newton and Manning (2002) suggested that the trends observed in Fig. 4 indicate that H_2O is not involved as a solution mechanism in the dissolution of the Ca salts. If it were, the rapidly decreasing H_2O activity associated with increasing NaCl mole fraction would inhibit mineral solubility in concentrated solutions, as is seen for silicates (quartz, wollastonite, grossular) and corundum (Newton and Manning, 2000, 2006, 2007). Instead, the rise in solubility with NaCl concentration points to interactions of Na^+ and Cl^- with the fluorapatite components to form complexes (e.g., $CaCl^+$, $NaPO_4^-$, CaF^+, etc.).

4.3. P–T dependence of solubility enhancement by NaCl

The relative enhancement of fluorapatite solubility by NaCl, as measured by the ratio X_{Ca}/X°_{Ca}, increases with increasing T (Fig. 5a). This behavior is similar to that of anhydrite and calcite (Newton and Manning, 2002, 2005). The opposite effect is seen with P (Fig. 5b), in that the relative solubility enhancement decreases as P increases. The same observation was made for fluorite by Tropper and Manning (2007b). This behavior is chiefly due to the very large increase in solubility with P in pure H_2O.

4.4. Implications for REE mobility

The nucleation of monazite as a reaction product in all of the experiments indicates that the LREE have relatively low solubility in H_2O–NaCl at the investigated conditions. On the other hand, the

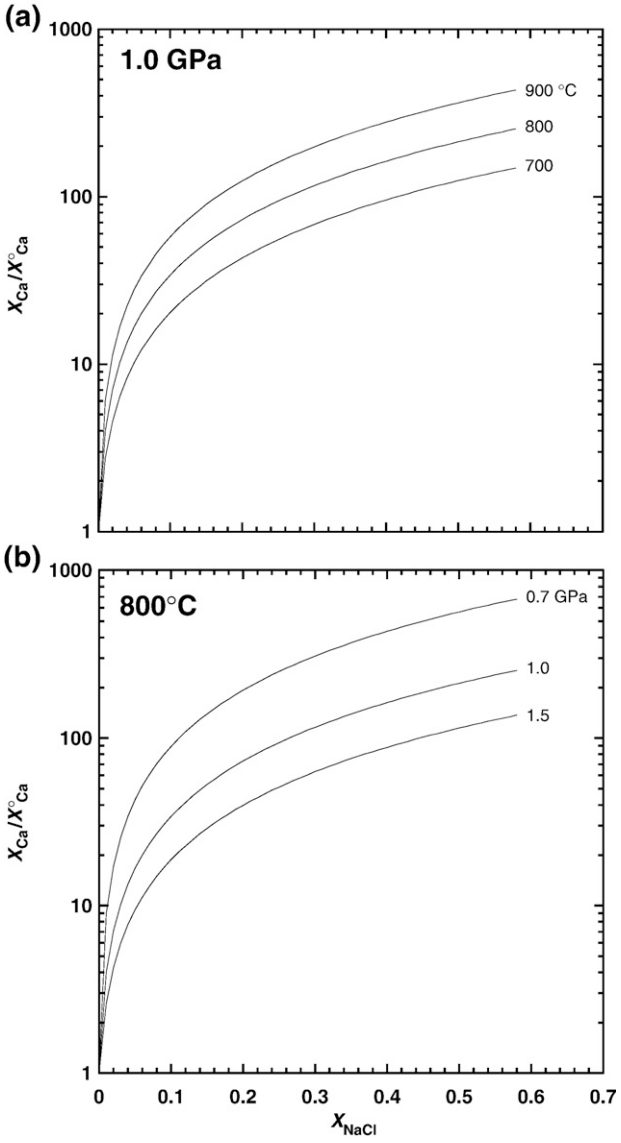

Fig. 5. Variation in fluorapatite solubility enhancement by NaCl with temperature at 1.0 GPa (a) and with pressure at 800 °C (b), as calculated from Eqs. (1)–(3).

negligible weight of monazite grains suggests that LREE are soluble to at least some degree. An upper bound on the solubility of LREE in fluorapatite-saturated H_2O–NaCl brines can be estimated by making three assumptions: (1) the maximum permissible residual monazite is present (i.e., 3σ above zero, or 0.6 μg); (2) residual fluorapatite is unzoned; and (3) LREE in the newly formed monazite are present in the same ratio as in Durango fluorapatite. Durango fluorapatite contains variable LREE, but analyses of Young et al. (1969) and Harlov and Förster (2003) provide plausible mean La, Ce, Pr and Nd concentrations of 3600±400, 4600±500, 470±40 and 1350±150 ppm, respectively. Fluorapatite solubility in pure H_2O is sufficiently low at all conditions that, under the stated assumptions, 0.6 mg of monazite would contain all LREE available from the dissolved fluorapatite. Thus, LREE solubility is not distinguishable from zero in pure H_2O. However, LREE solubility must be nonzero for all experiments containing NaCl. Assuming 0–0.6 μg of newly formed monazite in each experiment, total dissolved LREE would be up to ~250 ppm over the conditions of this study. The concentration of LREE in solution increases with X_{NaCl}, T, and P, as does fluorapatite. The results suggest that fluorapatite-fluid partition coefficient (D) for LREE decreases with increasing T, P, and X_{NaCl} in NaCl-bearing fluids, and the lowest value would be $D \approx 45$ at 900 °C, 1.5 GPa, and $X_{NaCl}=0.47$. The qualitative dependence of LREE concentration on X_{NaCl} implies strong REE complexing with Cl^- (and perhaps minor complexing with PO_4^{3-} and F^-), consistent with inferences from theory (Haas et al., 1995) and natural metamorphic settings (e.g., Gieré, 1990; Ague, 2003; Harlov et al., 2006; Hanson and Harlov, 2007). The results indicate that NaCl-rich brines can be powerful agents for REE metasomatism in high-P, high-T metasomatic settings.

5. Conclusions

(1) Durango fluorapatite dissolves incongruently in H_2O and H_2O–NaCl to monazite and solutes at the conditions of this study. The solubility of Durango fluorapatite in pure H_2O is quite low at 700–900 °C and 0.7–2.0 GPa. Addition of NaCl significantly enhances fluorapatite solubility at all P and T investigated.

(2) Our results differ from those of Ayers and Watson (1991) in three important ways. First, we found that fluorapatite solubility in pure H_2O is lower by about a factor of ~10 where the two studies overlap. In addition, our data indicate the opposite dependence on P and systematic increase with T. Finally, the new data indicate that fluorapatite solubility displays a strong dependence on NaCl concentration, whereas Ayers and Watson (1991) found none. We propose that the discrepancies between the studies are due to the unrecognized growth of vapor-transport crystals in the earlier work.

(3) Compared to calcite, fluorite or anhydrite solubility in pure H_2O and H_2O–NaCl, fluorapatite solubility is significantly lower at a given P, T and X_{NaCl} in the range investigated. Fluorapatite is therefore more refractory than other minor Ca salts found in crustal and mantle rocks. Notably, however, its solubility shows a stronger enhancement with the addition of NaCl than does fluorite or calcite.

(4) Crude estimates of the solubility of LREE in fluorapatite-equilibrated fluids suggest that the concentration of these elements is significantly enhanced by NaCl addition. This finding suggests complexing chiefly as chlorides and indicates that LREE metasomatism can be expected for high-grade metamorphic rocks which interacted with saline brines.

Acknowledgements

This project was part of the Ph.D. dissertation of the senior author. Support was provided by the University of California Los Angeles, a Mineralogy and Petrology Research Grant from the Mineralogical Society of America, and National Science Foundation grants EAR-0337170 and 0711521. We thank Robert C. Newton for assistance and advice. The manuscript was improved by insightful reviews by J. Walther and D. Harlov.

References

Ague, J.J., 2003. Fluid infiltration and transport of major, minor, and trace elements during regional metamorphism of carbonate rocks, Wepawaug Schist, Connecticut, USA. American Journal of Science 303, 753–816.
Aranovich, L.Y., Newton, R.C., 1996. H_2O activity in concentrated NaCl solutions at high pressures and temperatures measured by the brucite-periclase equilibrium. Contributions to Mineralogy and Petrology 125, 200–212.
Ayers, J.C., Watson, E.B., 1991. Solubility of apatite, monazite, zircon, and rutile in supercritical aqueous fluids with implications for subduction zone geochemistry. Philosophical Transactions of the Royal Society of London Series A 335, 365–375.
Ayers, J.C., Watson, E.B., 1993a. Apatite/fluid partitioning of rare-earth elements and strontium — experimental results at 1.0 GPa and 1000 °C and application to models of fluid–rock interaction. Chemical Geology 110, 299–314.
Ayers, J.C., Watson, E.B., 1993b. Rutile solubility and mobility in supercritical aqueous fluids. Contributions to Mineralogy and Petrology 114, 321–330.
Ayers, J.C., Brenan, J.B., Watson, E.B., Wark, D.A., Minarik, W.G., 1992. A new capsule technique for hydrothermal experiments using the piston-cylinder apparatus. American Mineralogist 77, 1080–1086.
Barnicoat, A.C., 1988. The mechanism of veining and retrograde alteration of Alpine eclogites. Journal of Metamorphic Geology 6, 545–558.
Bebout, G.E., Barton, M.D., 1993. Metasomatism during subduction — products and possible paths in the Catalina Schist, California. Chemical Geology 108, 61–92.
Boyce, J.W., Hervig, R.L., 2008. Magmatic degassing histories from apatite volatile stratigraphy. Geology 36, 63–66.
Caciagli, N.C., Manning, C.E., 2003. The solubility of calcite in water at 6–16 kbar and 500–800 degrees C. Contributions to Mineralogy and Petrology 146, 275–285.
Farley, K.A., Stockli, D.F., 2002. (U–Th)/He dating of phosphates: apatite, monazite, and xenotime. Reviews in Mineralogy and Geochemistry 48, 559–577.
FernandezCaliani, J.C., Casquet, C., Galan, E., 1996. Complex multiphase fluid inclusions in wollastonite from the Merida contact-metamorphic deposit, Spain: evidence for rock/HCl-rich fluid interaction. European Journal of Mineralogy 8, 1015–1026.
Fleet, M.E., Pan, Y.M., 1995a. Site preference of rare earth elements in fluorapaptite. American Mineralogist 80, 329–335.
Fleet, M.E., Pan, Y.M., 1995b. Crystal chemistry of rare earth elements in fluorapatite and some calc-silicates. European Journal of Mineralogy 7, 591–605.
Fleischer, M., Altschuler, Z.S., 1986. The lanthanides and yttrium in minerals of the apatite group — an analysis of the available data. Neues Jahrbuch für Mineralogie Monatschefte 10, 467–480.
Franz, L., Romer, R.L., Klemd, R., Schmid, R., Oberhänsli, R., Wagner, T., Shuwen, D., 2001. Eclogite-facies quartz veins within metabasites of the Dabie Shan (eastern China): pressure–temperature–time–deformation path, composition of the fluid phase and fluid flow during exhumation of high-pressure rocks. Contributions to Mineralogy and Petrology 141, 322–346.
Gao, J., Klemd, R., 2001. Primary fluids entrapped at blueschist to eclogite transition: evidence from the Tianshan meta-subduction complex in northwestern China. Contributions to Mineralogy and Petrology 142, 1–14.
Gao, J., John, T., Klemd, R., Xiong, X.M., 2007. Mobilization of Ti–Nb–Ta during subduction: Evidence from rutile-bearing dehydration segregations and veins hosted in eclogite, Tianshan, NW China. Geochimica et Cosmochimica Acta 71, 4974–4996.
Giaramita, M.J., Sorensen, S.S., 1994. Primary fluids in low-temperature eclogites — evidence from two subduction complexes (Dominican Republic, and California, USA). Contributions to Mineralogy and Petrology 117, 279–292.
Gieré, R., 1990. Hydrothermal mobility of Ti, Zr, and REE: examples from the Bergell and Adamello contact aureoles (Italy). Terra Nova 2, 60–67.
Gleadow, A.G.W., Belton, D.X., Kohn, B.P., Brown, R.W., 2002. Fission track dating of phosphate minerals and the thermochronology of apatite. Reviews of Mineralogy and Geochemistry 48, 579–630.
Glodny, J., Austrheim, H., Molina, J.F., Rusin, A.I., Seward, D., 2003. Rb/Sr record of fluid–rock interaction in eclogites: the Marun–Keu complex, Polar Urals, Russia. Geochimica et Cosmochimica Acta 67, 4353–4371.
Gromet, L.P., Silver, L.T., 1983. Rare-earth element distributions among minerals in a granodiorite and their petrogenetic implications. Geochimica et Cosmochimica Acta 47, 925–939.
Haar, L., Gallagher, J.S., Kell, G.S., 1984. NBS/NRC Steam Tables. Hemisphere, New York.
Haas, J.R., Shock, E.L., Sasani, D.C., 1995. Rare earth elements in hydrothermal systems: estimates of standard partial molal thermodynamic properties of aqueous complexes of the rare earth elements at high pressures and temperatures. Geochimica et Cosmochimica Acta 59, 4329–4350.
Hanson, E.C., Harlov, D.E., 2007. Whole-rock, phosphate, and silicate compositional trends across an amphibolite- to granulite-facies transition, Tamil Nadu, India. Journal of Petrology 48, 1641–1680.
Harlov, D.E., Förster, H.J., 2002. High-grade fluid metasomatism on both a local and a regional scale: the Seward Peninsula, Alaska, and the Val Strona di Omegna, Ivrea–Verbano zone, northern Italy. Part II: phosphate mineral chemistry. Journal of Petrology 43, 801–824.
Harlov, D.E., Förster, H.J., 2003. Fluid-induced nucleation of (Y+REE)-phosphate minerals within apatite: nature and experiment. Part II. Fluorapatite. American Mineralogist 88, 1209–1229.
Harlov, D.E., Förster, H.J., Nijland, T.G., 2002. Fluid-induced nucleation of (Y+REE)-phosphate minerals within apatite: nature and experiment. Part I. Chlorapatite. American Mineralogist 87, 245–261.

Harlov, D.E., Wirth, R., Förster, H.J., 2005. An experimental study of dissolution–reprecipitation in fluorapatite: fluid infiltration and the formation of monazite. Contributions to Mineralogy and Petrology 150, 268–286.
Harlov, D.E., Johansson, L., Van den Kerkhof, A., Förster, H.-J., 2006. The role of advective fluid flow and diffusion during localized, solid-state dehydration: Söndrum Stenhuggeriet, Halmstad, SW Sweden. Journal of Petrology 47, 3–33.
Harrison, T.M., Catlos, E.J., Montel, J.-M., 2002. U–Th–Pb dataing of phosphate minerals. Reviews in Mineralogy and Geochemistry 48, 523–558.
Korzhinskiy, M.A., 1981. Apatite solid solutions as indicators of the fugacity of HCl° and HF° in hydrothermal fluids. Geochemistry International 18, 44–60.
Koster van Groos, A.F., 1991. Differential thermal analysis of the liquidus relations in the system NaCl–H_2O to 6 kbar. Geochimica et Cosmochimica Acta 55, 2811–2817.
Manning, C.E., 1994. The solubility of quartz in H_2O in the lower crust and upper mantle. Geochimica et Cosmochimica Acta 58, 4831–4839.
Manning, C.E., 1998. Fluid composition at the blueschist–eclogite transition in the model system Na_2O–MgO–Al_2O_3–SiO_2–H_2O–HCl. Swiss Bulletin of Mineralogy and Petrology 78, 225–242.
Manning, C.E., Boettcher, S.L., 1994. Rapid-quench hydrothermal experiments at mantle pressures and temperatures. American Mineralogist 79, 1153–1158.
Nagasawa, H., 1970. Rare earth concentrations in zircons and apatites and their host dacites and granites. Earth and Planetary Science Letters 9, 359–364.
Nash, W.P., Hausel, W.D., 1973. Partial pressures of oxygen, phosphorous and fluorine in some lunar lavas. Earth and Planetary Science Letters 20, 13–27.
Newton, R.C., Manning, C.E., 2000. Quartz solubility in concentrated aqueous NaCl solutions at deep crust–upper mantle metamorphic conditions: 2–15 kbar and 500–900 °C. Geochimica et Cosmochimica Acta 64, 2993–3005.
Newton, R.C., Manning, C.E., 2002. Experimental determination of calcite solubility in H_2O–NaCl solutions at deep crust/upper mantle pressures and temperatures: implications for metasomatic processes in shear zones. American Mineralogist 87, 1401–1409.
Newton, R.C., Manning, C.E., 2005. Solubility of anhydrite, $CaSO_4$, in NaCl–H_2O solutions at high pressures and temperatures: applications to fluid–rock interaction. Journal of Petrology 46, 701–716.
Newton, R.C., Manning, C.E., 2006. Solubilities of corundum, wollastonite and quartz in H_2O–NaCl solutions at 800 °C and 10 kbar: interaction of simple minerals with brines at high pressure and temperature. Geochimica et Cosmochimica Acta 70, 5571–5582.
Newton, R.C., Manning, C.E., 2007. Solubility and stability of grossular, $Ca_3Al_2Si_3O_{12}$, in the system $CaSiO_3$–Al_2O_3–NaCl–H_2O at 800 °C and 10 kbar. Geochimica et Cosmochimica Acta 71, 5191–5202.
O'Reilly, S.Y., Griffin, W.L., 2000. Apatite in the mantle: implications for metasomatic processes and high heat production in Phaerozoic mantle. Lithos 53, 217–232.
Pan, Y.M., Fleet, M.E., 1996. Rare earth element mobility during prograde granulite facies metamorphism: significance of fluorine. Contributions to Mineralogy and Petrology 123, 251–262.
Pan, Y.M., Fleet, M.E., 2002. Compositions of the apatite-group minerals: substitution mechanisms and controlling factors. Reviews in Mineralogy and Geochemistry 48, 13–49.
Patiño Douce, A.E., Roden, M., 2006. Apatite as a probe of halogen and water fugacities in the terrestrial planets. Geochimica et Cosmochimica Acta 70, 3173–3196.
Philippot, P., Selverstone, J., 1991. Trace-element-rich brines in eclogitic veins — implications for fluid composition and transport during subduction. Contributions to Mineralogy and Petrology 106, 417–430.
Piccoli, P.M., Candela, P.A., 1994. Apatite in felsic rocks: a model for the estimation of initial halogen concentrations in the Bishop Tuff (Long Valley) and Tuolmne Intrusive Suite (Sierra Nevada Batholith) magmas. American Journal of Science 294, 92–135.
Piccoli, P.M., Candela, P.A., 2002. Apatite in igneous systems. Reviews in Mineralogy and Geochemistry 48, 255–292.
Rubatto, D., Hermann, J., 2003. Zircon formation during fluid circulation in eclogites (Monviso, Western Alps): implications for Zr and Hf budget in subduction zones. Geochimica et Cosmochimica Acta 67, 2173–2187.
Selverstone, J., Franz, G., Thomas, S., Getty, S., 1992. Fluid variability in 2-GPa eclogites as an indicator of fluid behavior during subduction. Contributions to Mineralogy and Petrology 112, 341–357.
Sorensen, S.S., Grossman, J.N., 1989. Enrichment of trace-elements in garnet amphibolites from a paleo-subduction zone — Catalina Schist, Southern-California. Geochimica et Cosmochimica Acta 53, 3155–3177.
Spear, F.S., Pyle, J.M., 2002. Apatite, monazite, and xenotime in metamorphic rocks. Reviews in Mineralogy and Geochemistry 48, 293–335.
Torok, K., 2001. Multiple fluid migration events in the Sopron Gneisses during the Alpine high-pressure metamorphism, as recorded by bulk-rock and mineral chemistry and fluid inclusions. Neues Jahrbuch Für Mineralogie. Abhandlungen 177, 1–36.
Tropper, P., Manning, C.E., 2005. Very low solubility of rutile in H_2O at high pressure and temperature, and its implications for Ti mobility in subduction zones. American Mineralogist 90, 502–505.
Tropper, P., Manning, C.E., 2007a. The solubility of corundum in H_2O at high pressure and temperature and its implications for Al mobility in the deep crust and upper mantle. Chemical Geology 240, 54–60.
Tropper, P., Manning, C.E., 2007b. The solubility of fluorite in H_2O and H_2O–NaCl at high pressure and temperature. Chemical Geology 242, 299–306.
Wyllie, P.J., Cox, K.G., Biggar, G.M., 1962. The habit of apatite in synthetic systems and igneous rocks. Journal of Petrology 3, 238–243.
Xu, J.H., Xie, Y.L., Li, J.P., Hou, Z.Q., 2001. Discovery of Sr-bearing and LREE daughter minerals in fluid inclusions of Maoniuping REE deposit, Sichuan Province. Progress in Natural Science 11, 833–837.
Yardley, B.W.D., 1985. Apatite composition and fugacities of HF and HCl in metamorphic fluids. Mineralogical Magazine 49, 77–79.
Young, E.J., Myers, A.T., Munson, E.L., Conklin, N.M., 1969. Mineralogy and geochemistry of fluorapatite from Cerro de Mercado, Durango, Mexico. U.S. Geological Survey Professional Paper 650-D, 84–93.
Zhu, C., Sverjensky, D.A., 1991. Partitioning of F–Cl–OH between minerals and hydrothermal fluids. Geochimica et Cosmochimica Acta 55, 1837–1858.
Zhu, C., Sverjensky, D.A., 1992. F–Cl–OH partitioning between biotite and apatite. Geochimica et Cosmochimica Acta 56, 3435–3467.